Inorganic Chemistry

Article

pubs.acs.org/IC

Origin of Small Barriers in Jahn–Teller Systems: Quantifying the Role of 3d–4s Hybridization in the Model System NaCl:Ni$^+$

M. T. Barriuso,*[†] B. Ortiz-Sevilla,[†] J. A. Aramburu,[‡] P. García-Fernández,[‡] J. M. García-Lastra,[§] and M. Moreno[‡]

[†]Departamento de Física Moderna and [‡]Departamento de Ciencias de la Tierra y Física de la Materia Condensada, Universidad de Cantabria, Avenida de los Castros s/n, 39005 Santander, Spain

[§]Center for Atomic-Scale Materials Design, Department of Physics, Technical University of Denmark, DK-2800 Kongens Lyngby, Denmark

Supporting Information

ABSTRACT: Despite its relevance, the microscopic origin of the energy barrier, B, between the compressed and elongated geometries of Jahn–Teller (JT) systems is not well understood yet because of a lack of quantitative data about its various contributions. Seeking to clear up this matter, we have carried out both periodic and cluster ab initio calculations on the model system NaCl:Ni$^+$. This system is particularly puzzling because, according to experimental data, its barrier is much smaller than that for other d^9 and d^7 ions in similar lattices. All calculations performed on the model system lead, in fact, to values $|B| \leq 160$ cm^{-1}, which are certainly smaller than $B = 500$ cm^{-1} derived for NaCl:M^{2+} (M = Ag, Rh) or $B = 1024$ cm^{-1} obtained for KCl:Ag^{2+}. As a salient feature, analysis of calculations carried out as a function of the Q_θ ($\sim 3z^2 - r^2$) coordinate unveils the microscopic origin of the barrier. It is quantitatively proven that the elongated geometry observed for NaCl:Ni$^+$ is due to the 3d–4s vibronic admixture, which is slightly larger than the anharmonicity in the e_g JT mode that favors a compressed geometry. The existence of these two competing mechanisms explains the low value of B for the model system, contrary to cases where the complex formed by d^9 or d^7 ions is elastically decoupled from the host lattice. Although the magnitude of B for NaCl:Ni$^+$ is particularly small, the tunneling splitting, 3Γ, is estimated to be below 9 cm^{-1}, thus explaining why the coherence is easily destroyed by random strains and thus a static JT effect is observed experimentally. As a main conclusion, the barrier in JT systems cannot be understood neglecting the tiny changes of the electronic density involved in small distortions. The present calculations reasonably explain the experimental **g** tensor of NaCl:Ni$^+$, pointing out that the d–d transitions in $NiCl_6^{5-}$ are much smaller than those for $CuCl_6^{4-}$ and the optical electronegativity of Ni$^+$ is only around 1.

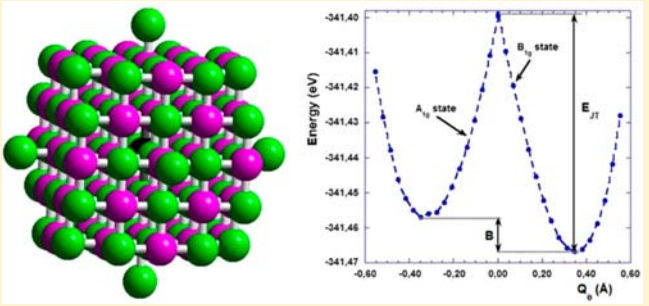

1. INTRODUCTION

A fundamental question to be answered in the research of materials is the actual origin of their structure and its relationship with the arrangement of electronic levels. To gain better insight into this relevant matter is certainly not easy because compounds that are similar in composition do not always display the same structure. For instance, at low temperatures, $KMgF_3$ and $KNiF_3$ perovskites are both cubic, while $KMnF_3$ is tetragonal.[1,2] In the same vein, there is a striking difference in the geometry of the $CuCl_4(NH_3)_2^{2-}$ and $CuCl_4(H_2O)_2^{2-}$ centers formed, for example, in Cu^{2+}-doped NH_4Cl. While the first center is tetragonal with four equivalent equatorial Cl^- ligands, the substitution of *axial* NH_3 molecules by another neutral molecule, H_2O, produces a big orthorhombic distortion in the *equatorial* plane.[3−6] Despite these facts, to understand what among two or more possible phases of a compound becomes the most stable at low temperatures is not a simple question because energy differences on the order of 100 cm^{-1} or below are often involved.[2,6−8]

A situation of this kind is found in the realm of the $E_g \otimes e_g$ Jahn–Teller (JT) effect[9−12] widely studied in the case of d^9 and d^7 ions in cubic insulating lattices under octahedral coordination. In these cases, the dependence of the ground-state energy as a function of Q_θ ($\sim 3z^2 - r^2$) and Q_ε ($\sim x^2 - y^2$) coordinates exhibits three equivalent adiabatic minima, involving tetragonal distortions along the three main axes, which are separated by an energy barrier B (Figure 1). This barrier plays a key role for understanding the properties of JT systems. In fact, the existence of a low barrier is a necessary condition for observing coherent tunneling among the different minima in electron paramagnetic resonance (EPR) experiments, a phenomenon termed the dynamic JT effect.[9−14] By contrast, as often happens, the unavoidable random strains, present in any real crystal, destroy the coherence, giving rise to the static JT effect.[9,13,14] In this case, the *sign* of B determines

Received: April 11, 2013
Published: July 29, 2013

   dx.doi.org/10.1021/ic4009009 | Inorg. Chem. 2013, 52, 9338–9348

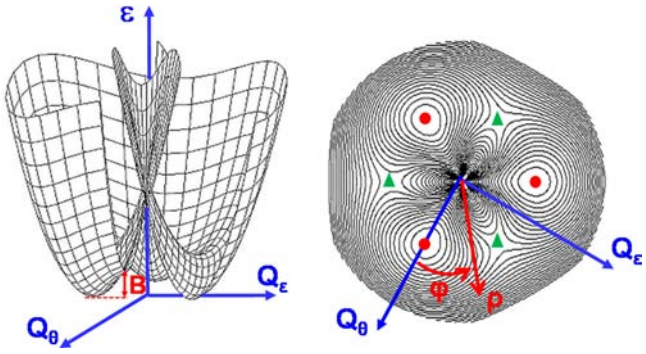

Figure 1. Left: "Tricorn" or warped "Mexican hat" corresponding to the adiabatic potential energy surface of the $E_g \otimes e_g$ JT effect showing the energy barrier *B*. Right: Top view of the "tricorn" showing the positions of three minima (red circles) and three saddle points (green triangles).

whether the equilibrium geometry corresponds to an elongated or a compressed octahedron and thus the electronic ground state. So, if in the warped surface depicted in Figure 1, the minima describe an elongated conformation and the saddle points correspond to a compressed one, $B > 0$, while the reverse happens if $B < 0$. Accordingly, if $B > 0$, the electronic ground state is B_{1g} for a d^9 ion and A_{1g} for a d^7 ion. Furthermore, in a static JT effect, the barrier controls the rate of incoherent transitions among the three wells and thus the passage of a tetragonal EPR spectrum to an isotropic one when the temperature is raised.[9,10,12]

Despite its relevance, little is still known on the actual values of *B* for JT systems and the microscopic origin of the energy barrier. This work is devoted to improve our *quantitative* knowledge on this matter by exploring in some detail the origin of *B* for the model system NaCl:Ni^+.[15] This system has been chosen for the following reasons: (i) The low temperature, T_t = 35 K, at which the static EPR spectrum[15] of NaCl:Ni^+ in the X band starts to disappear suggests that its barrier, *B*, is clearly smaller than that for other d^9 (Ag^{2+}, Cu^{2+})[16,17] and d^7 (Rh^{2+})[18] ions in the *same* host lattice, a surprising fact that deserves to be explored. (ii) Despite the small *B* value expected for NaCl:Ni^+, the low-temperature EPR spectra clearly prove that the JT effect is static and not dynamic.[15] (iii) It has been shown[11] that the *vibronic* 4d−5s admixture for NaCl:Rh^{2+} makes an important, though not dominant, contribution to *B*. As the *n*d−(*n*+1)s separation is reduced upon passing from a divalent to a monovalent cation,[19] the effects of the vibronic *n*d−(*n*+1)s admixture on *B* are expected to be enhanced in a system like NaCl:Ni^+.

It was earlier argued by Öpik and Pryce[20] that the barrier in a JT system is due to the anharmonicity present in the e_g vibration mode. Accordingly, a MX_6 complex (M = d^9 or d^7 ion) embedded in an insulating cubic lattice would prefer an elongated over a compressed geometry *provided* that it is elastically decoupled from the rest of the lattice where it is embedded.[11,21] By contrast, other authors[12,22,23] have ascribed the origin of *B* to the quadratic JT term involving *operators* that depend quadratically on Q_θ and Q_ε coordinates. However, a previous *quantitative* study performed on several JT systems points out that the quadratic JT term plays a minor role while the vibronic admixture of e_g* orbitals ($\sim 3z^2 - r^2$; $\sim x^2 - y^2$) with other ones due to the *linear* JT term but treated in *second-order* perturbations yields an *important* contribution[11] to *B*. More precisely, in NaCl:Rh^{2+}, about 40% of the barrier has been shown to come from the vibronic admixture of the a_{1g}*($\sim 3z^2$-r^2) orbital with the mainly 5s level of Rh^{2+}, although the dominant contribution does arise from the anharmonicity.[11] Moreover, because the $RhCl_6^{4-}$ complex in NaCl is elastically decoupled from the rest of the lattice, *both* contributions have been shown[11,13,14] to favor an elongated geometry, making B = 511 cm^{-1}. These results explain our interest in Ni^+ systems because the 3d−4s separation is only 2 eV for the free ion while values close to 10 eV correspond to the 4d−5s separation for free Ag^{2+} or Rh^{2+} ions.[19] The influence of the 3d−4s mixing on the equilibrium geometry of Cu^{2+} complexes has previously been suggested by several authors.[24−28]

Although Ni^+ is an unusual oxidation state for nickel, such a valence has been stabilized in lattices like LiF,[29] NaF,[29] $KZnF_3$,[30] $KMgF_3$,[31] $CsCaF_3$,[32] or AgCl[33,34] initially doped with Ni^{2+} and subsequently irradiated with X-rays or UV rays. Nevertheless, in Bridgman-grown crystals of NaCl doped with divalent nickel, EPR experiments by Shengelaya et al.[15] have undoubtedly proven the formation of Ni^+ impurities *without* irradiating the samples. Such impurities are likely formed through chemical reactions at a temperature of ∼1100 K during the purification process of the molten salt.[15] This is the reason why the Ni^+ ions formed in this way easily replace a host Na^+ cation in the NaCl lattice without having a close vacancy. Thus, at variance with what happens for LiF:Ni^+,[29] $KMgF_3$:Ni^+,[31] or $CsCaF_3$:Ni^+,[32] *only one* Ni^+ center is formed in the samples of NaCl:Ni^+ explored by Shengelaya et al.[15] This is thus an important reason for choosing NaCl:Ni^+ among the different JT systems involving Ni^+.

The **g** tensor of NaCl:Ni^+ measured at T = 20 K ($g_\parallel$ = 2.86; $g_\perp$ = 2.10) undoubtedly proves[15] that the equilibrium geometry corresponds to an elongated octahedron, although no precise information on the equilibrium R_{ax} and R_{eq} values can be derived from it. However, this static spectrum starts to disappear at T_t = 35 K in the X band, while an isotropic spectrum with g = 2.40 is already observed at 55 K.[15] Thus, both the low value of T_t and the high value of $g_\parallel - g_\perp$ strongly suggest that the barrier between two equivalent distortions is certainly small because *B* is roughly proportional[9,35] to $T_t/L(g_\parallel - g_\perp)$. For comparison, in NaCl:Ag^{2+}, where $g_\parallel$ = 2.198 and $g_\perp$ = 2.041,[16,10] T_t = 95 K, while the calculated *B* value is equal[35] to 500 cm^{-1}. In KCl:Ag^{2+}, whose **g** tensor is very close to that measured for NaCl:Ag^{2+}, it is found[35] that B = 1024 cm^{-1}, which is consistent with a higher T_t = 160 K value.[16]

Bearing these facts in mind, the present work is addressed to explore the system NaCl:Ni^+ by means of ab initio calculations based on density functional theory (DFT), together with an analysis of the results, seeking to clarify the mechanisms responsible for the energy barrier. In particular, aside from determining the equilibrium geometry, we want to understand quantitatively why the barrier in NaCl:Ni^+[15] is seemingly much smaller than that for Ag^{2+},[16] Cu^{2+},[17] or Rh^{2+}[18,36] impurities in the *same* lattice. For achieving these goals, first-principles calculations using periodic supercells as well as finite clusters have both been carried out. Because of the expected smallness of *B* for NaCl:Ni^+, different types of calculations are used in order to see if all of them are consistent with this view.

It should be noted that, because the 3d−4s separation for free Ni^+ (2 eV) is much smaller than that for divalent d^9 ions like Cu^{2+} or Ag^{2+},[19] the more *diffuse* 4s levels can play an important role for understanding the properties of NaCl:Ni^+. For this reason, that system is, in principle, more complicated

dx.doi.org/10.1021/ic4009009 | *Inorg. Chem.* 2013, 52, 9338−9348

than those involving divalent or trivalent transition-metal impurities.

This work is arranged as follows. Details on the calculation procedure are given in section 2, while the main results obtained in the present work are shown in section 4. In that section, particular attention is paid to exploring the energy, $E(A_{1g})$ and $E(B_{1g})$, of *both* A_{1g} and B_{1g} electronic states as a function of the Q_θ coordinate. Seeking to clear out the mechanism responsible for the barrier, B, in NaCl:Ni^+, such dependencies are analyzed following the procedure[11] employed in an analysis of cluster calculations on NaCl:Rh^{2+}. For the sake of completeness, a recall of that procedure is previously given in section 3.

2. COMPUTATIONAL DETAILS

2.1. Periodic Calculations. Periodic ab initio calculations based on DFT have been carried out on the NaCl:Ni^+ system in order to obtain the optimized geometries of the tetragonal elongated and compressed conformations of the JT center and thus the energy barrier between them. All calculations have been performed on 2 × 2 × 2 conventional supercells (which comprise 64 ions), where the Ni^+ impurity replaces a Na^+ ion of the lattice.

Most calculations were performed with the *CRYSTAL09* package that employs localized Gaussian-type orbital (GTO) basis sets to represent the Bloch orbitals.[37] Because the energy barrier, B, between elongated and compressed conformations of the $NiCl_6^{5-}$ complex in NaCl is expected to be very small, basis sets of different qualities as well as various exchange-correlation functionals have been employed. With regard to the basis sets, most of the calculations have been performed using the pob-TZVP-2012 functions, recently optimized by Peintinger, Vilela Oliveira, and Bredow,[38] which are all-electron with triple-ζ valence with polarization quality. For the sake of comparison, other basis sets of lesser quality have also been used,[39−41] which can be taken from the *CRYSTAL* database.[42] Concerning the exchange-correlation functionals, we have used the following ones: Perdew−Zunger parametrization of the Ceperley−Alder free-electron gas correlation results in the local density approximation[43] (LDA); a PBEsol functional designed specifically to improve the generalized gradient approximation (GGA) in solids.[44] Apart from these, we have also employed hybrid functionals (with respectively 16% and 20% of Hartree−Fock exchange) such as the B1WC[45] and PW1PW.[46] These hybrid functionals allow one to obtain geometries, band gaps, and thermochemistry properties with great accuracy and reliability without the need for semiempirical parameters like in DFT+U procedures.

We have employed a 4 × 4 × 4 k-point mesh, and the structures have been relaxed until a maximum force value below 0.02 eV/Å and a total energy change below 10^{-7} eV was obtained. It is worth noting that, contrary to what is usually found, the periodic calculations on NaCl:Ni^+ made with LDA and GGA functionals converge very slowly and thus are much more expensive than those performed with hybrid functionals.

For checking the reliability of the calculations, the equilibrium lattice parameter, a, and band gap, E_g, of pure NaCl have first been computed using the previously indicated basis sets and functionals. The results are compared with the experimental values[47] extrapolated to T = 0 K, a = 5.57 Å, and E_g = 8.5 eV.[48] As usual,[49] LDA and GGA-PBEsol methods systematically underestimate the a and E_g values, while the best results are found using the B1WC hybrid functional and the basis sets of higher quality, pob-TZVP-2012, a = 5.56 Å and E_g = 7.8 eV.

Additional geometry optimizations were carried out by means of the *Quantum-Espresso* code,[50] which uses delocalized plane waves as basis set functions. The kinetic energy cutoff for the wave functions was 40 hartree. The exchange-correlation energy has been computed with the GGA-Perdew−Burke−Ernzerhof (PBE) functional,[51] using ultrasoft pseudopotentials. The k-point grid was reduced to just the Γ point, although we have verified that with and increase in the grid, the results do not change. The structures were relaxed until a maximum force value below 0.03 eV/Å.

2.2. Cluster Calculations. We have also carried out DFT calculations using the cluster approximation. Calculations have been performed by means of the Amsterdam Density Functional (ADF) code,[52] version 2010, on clusters of 39, 87, and 123 atoms. To check the reliability of the present results, calculations have been performed using different exchange-correlation functionals. Among others, we have employed the Becke−Perdew (BP86)[53,54] and the PBE[51] functionals in the GGA. Moreover, some spin-unrestricted calculations have been performed using the B3LYP hybrid functional[55] with 20% of Hartree−Fock exchange.

All atoms have been described through basis sets of TZP quality (tripe-ζ Slater-type orbitals plus one polarization function) given in the program database and large frozen core (1s−2p orbitals for Cl and Na and 1s−3p for Ni). In the case of the B3LYP hybrid functional, all-electron calculations have been carried out. In the geometry optimizations, the positions of all ions, except first-shell Cl^- ones and second neighbors Na^+ in ⟨100⟩ directions, have usually been kept at their lattice positions. To verify the reliability of this approximation, a calculation on a 123-ion cluster has been carried out, allowing relaxation of the 33 ions not belonging to the surface. We have verified that the relaxation of all ions lying outside the Cl^- ligands is always smaller than 1%.

In all cluster calculations, the effects of the Coulomb potential, $V_R(\mathbf{r})$, due to the rest of the lattice on the electrons in the cluster have been taken into account. Such a potential is calculated in a first step by means of the Ewald method and is reproduced in a second step by means of a set of point charges, lying outside the cluster and kept at their host lattice positions, whose values are fitted to reproduce the right $V_R(\mathbf{r})$ potential inside the cluster.[6,56] For instance, in the case of the cluster containing 87 atoms (Figure 2), nine ion shells lying outside the cluster, involving 218 point charges, have been employed to reproduce $V_R(\mathbf{r})$ in 2000 points inside a sphere containing the cluster. The values of all charges belonging to a given shell are taken to be the same. We have verified that the difference between the exact $V_R(\mathbf{r})$ potential, calculated through the Ewald method, and that derived using the nine shells of point charges is always smaller than 0.02%.

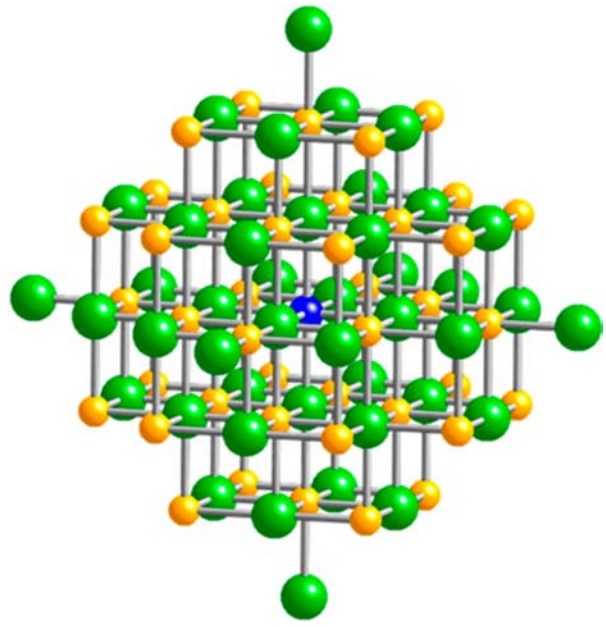

Figure 2. 87-atom cluster of NaCl:Ni^+ used in cluster calculations.

As a test of the reliability of the methodology used, the calculated value for the Na−Cl distance, R_0, for the pure NaCl lattice, using the GGA-BP86 exchange-correlation functional, was 2.824 Å, which differs

dx.doi.org/10.1021/ic4009009 | Inorg. Chem. 2013, 52, 9338−9348

by less than 1.4% from the experimental figure.[47] Similar results are found for the other cluster calculations.

More details on the cluster calculations, as well the optimized geometries, are shown in the Supporting Information.

3. ANALYSIS OF THE CALCULATED Q_θ DEPENDENCE OF $E(A_{1G})$ AND $E(B_{1G})$ ENERGIES

The physics of $E_g \otimes e_g$ JT systems is essentially driven by expansion of the Hamiltonian in terms of the Q_θ ($\sim 3z^2 - r^2$) and Q_ε ($\sim x^2 - y^2$) distortion coordinates[11]

$$H = H_0 + W_{1\theta}(\mathbf{r})\, Q_\theta + W_{1\varepsilon}(\mathbf{r})\, Q_\varepsilon + W_{2\theta}(\mathbf{r})\, (Q_\theta^2 - Q_\varepsilon^2) + W_{2\varepsilon}(\mathbf{r})\, (2Q_\theta Q_\varepsilon) + W_{2a}(\mathbf{r})\, (Q_\theta^2 + Q_\varepsilon^2) + W_{3a}(\mathbf{r})\, (Q_\theta^3 - 3Q_\theta Q_\varepsilon^2) + \ldots \quad (1)$$

Here H_0 is the adiabatic Hamiltonian for octahedral symmetry. The second and third terms describe the *linear* JT coupling, while those involving $W_{2\theta}(\mathbf{r})$ and $W_{2\varepsilon}(\mathbf{r})$ correspond to the second-order JT coupling. Because *operators* $W_{1\theta}(\mathbf{r})$ and $W_{2\theta}(\mathbf{r})$ transform like $3z^2 - r^2$ and $W_{1\varepsilon}(\mathbf{r})$ and $W_{2\varepsilon}(\mathbf{r})$ transform like $x^2 - y^2$, these terms act in a different way on the wave functions of the electronic doublet and thus have a vibronic character. By contrast, $W_{2a}(\mathbf{r})$ and $W_{3a}(\mathbf{r})$ belong to A_{1g} and the corresponding terms reflect the elastic and anharmonic contributions for the e_g mode, which are the *same* for the two wave functions of the electronic doublet.

When $Q_\varepsilon = 0$ and $Q_\theta \neq 0$, the octahedron is tetragonally deformed. The relationship between the Q_θ coordinate and the axial, R_{ax}, and equatorial, R_{eq}, metal−ligand distances of the distorted MX_6 complex is given by

$$Q_\theta = \frac{2}{\sqrt{3}}(R_{ax} - R_{eq}) \quad (2)$$

In an $E_g \otimes e_g$ JT problem, it is found that a minimum and a saddle point of the global energy surface can be found in the cross section where $Q_\varepsilon = 0$ (see Figure 1). In a previous work[11] analyzing the different factors contributing to the barrier, B, we showed that when the E_g term of an octahedral d^9 complex splits because of distortion in the Q_θ coordinate, the energy surfaces of the resulting A_{1g} and B_{1g} electronic states can be written as

$$E(A_{1g}) = V_{1e}Q_\theta + V_{2a}Q_\theta^2 + V_{3a}Q_\theta^3 + \{V_{2e} + V_{PJT}(A_{1g})\}Q_\theta^2 + \ldots \quad (3)$$

$$E(B_{1g}) = -V_{1e}Q_\theta + V_{2a}Q_\theta^2 + V_{3a}Q_\theta^3 + \{-V_{2e} + V_{PJT}(B_{1g})\}Q_\theta^2 + \ldots \quad (4)$$

The linear terms in eqs 3 and 4, involving the V_{1e} constant, come from the linear $W_{1\varepsilon}(\mathbf{r})$ JT operator in eq 1 using, in first-order perturbation, the *frozen* wave functions corresponding to the octahedral situation ($Q_\theta = Q_\varepsilon = 0$). The terms containing V_{2a} and V_{3a} come from the elastic and anharmonic contributions in eq 1, respectively. Because $Q_\theta > 0$ represents an elongated octahedron, the anharmonic term favors an elongated conformation when $V_{3a} < 0$. The contributions to eqs 3 and 4 involving V_{2e} arise from the second-order JT coupling in eq 1. With regard to the term $V_{PJT}(i)$ (i = A_{1g}, B_{1g}), it describes the energy lowering in the A_{1g} and B_{1g} states of the electronic doublet due to interaction with excited states through the *linear* JT operator in eq 1 in *second-order* perturbations. This mechanism of energy lowering is sometimes termed the pseudo-JT effect.[11,12]

If we only consider the excited states arising from the $e_g^2 4s^1$ configuration for NaCl:Ni^+, the difference between $V_{PJT}(A_{1g})$ and $V_{PJT}(B_{1g})$ can be understood by looking at Figure 3, taking

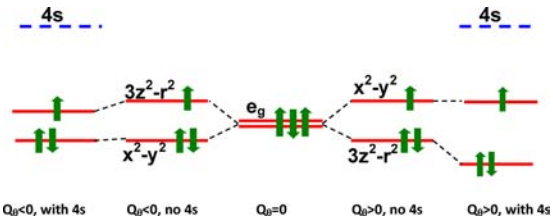

Figure 3. Pictorial description of the electronic ground state when $Q_\theta < 0$ and $Q_\theta > 0$. Because the close 4s level is coupled only to the $3d(3z^2-r^2)$ orbital, this vibronic mixing leads to a bigger decrease of the electronic energy for an elongated octahedron than for a compressed one.

into account that the 4s orbital can *only* be coupled to the $3z^2 - r^2$ one through the $W_{1\theta}(\mathbf{r})$ operator. As in the B_{1g} state there are two electrons in the $a_{1g}^*(\sim 3z^2-r^2)$ orbital and only one in the A_{1g} state (Figure 3) the energy gain due to this mechanism for B_{1g} is essentially twice that for A_{1g}.

$$V_{PJT}(B_{1g}) = 2V_{PJT}(A_{1g}) = V_{ds} \quad (5)$$

$$V_{ds} \cong -\frac{|\langle \phi_0(3z^2 - r^2)|W_{1\theta}(\mathbf{r})|\phi_0(4s)\rangle|^2}{\Delta_{ds}} \quad (6)$$

Here $\Delta_{ds} > 0$ means the energy difference between the mainly 4s orbital and $a_{1g}^*(\sim 3z^2-r^2)$ when $R_{eq} = R_{ax}$. Therefore, the $3d(3z^2-r^2)-4s$ vibronic mixing favors a B_{1g} ground state and thus an elongated geometry. It should be noted that, according to eqs 3−6, the vibronic $3d(3z^2-r^2)-4s$ mixing induces a *softening* of the force constant especially for the B_{1g} state. Generally, vibronic interactions are responsible for the *softening* of a force constant, K, in the electronic ground state. If $K < 0$ for a nonsymmetric vibration, the structure is no longer stable.[2,6,12,21,57]

To obtain reliable values of the quantities involved in eqs 3 and 4, it is useful to deal with the $[E(A_{1g}) + E(B_{1g})]/2$ and $[E(A_{1g}) - E(B_{1g})]/2$ quantities[11] whose expressions, according to eqs 3 and 4, are given by

$$\frac{E(A_{1g}) + E(B_{1g})}{2} = V_{2a}^{eff}Q_\theta^2 + V_{3a}Q_\theta^3 \quad (7)$$

$$\frac{E(A_{1g}) - E(B_{1g})}{2} = V_{1e}Q_\theta - V_{2e}^{eff}Q_\theta^2 \quad (8)$$

$$V_{2a}^{eff} = V_{2a} + \frac{3}{2}V_{ds} \quad (9)$$

$$V_{2e}^{eff} = -V_{2e} + \frac{1}{2}V_{ds} \quad (10)$$

If, for instance, the equilibrium geometry of the MX_6 complex ($M = d^9$ ion) placed in a cubic lattice is elongated, there are three equivalent distortions characterized by $\{Q_\theta = \rho_E;\ Q_\varepsilon = 0\}$, $\{Q_\theta = -(1/2)\rho_E;\ Q_\varepsilon = \sqrt{3}/2\rho_E\}$, and $\{Q_\theta = -(1/2)\rho_E;\ Q_\varepsilon = -\sqrt{3}/2\rho_E\}$. The energy barrier, B, between two equivalent distortions is just given by the energy difference of a

dx.doi.org/10.1021/ic4009009 | Inorg. Chem. 2013, 52, 9338−9348

compressed complex at its equilibrium geometry (at $\{Q_\theta = -\rho_C;\ Q_\varepsilon = 0\}$) and that corresponding to an elongated one computed at $\{Q_\theta = \rho_E;\ Q_\varepsilon = 0\}$. Thus, according to eqs 3 and 4, B is given by

$$\begin{aligned} B &= E(A_{1g};\ \rho = -\rho_C) - E(B_{1g};\ \rho = \rho_E) \\ &= -V_{1e}(\rho_C - \rho_E) + V_{2a}({\rho_C}^2 - {\rho_E}^2) - V_{3a}({\rho_C}^3 + {\rho_E}^3) \\ &\quad - V_{ds}(2{\rho_E}^2 - {\rho_C}^2) + V_{2e}({\rho_E}^2 + {\rho_C}^2) \end{aligned} \tag{11}$$

Therefore, if $\rho_C = \rho_E$, the barrier is determined by the anharmonic term and those involving V_{ds} and V_{2e}. It has previously been shown[11] that V_{2e} is negligible with respect to the pseudo-JT contribution in eqs 3 and 4. Moreover, if in the present case the pseudo-JT coupling is overwhelmingly dominated by the $3d(3z^2-r^2)-4s$ vibronic mixing, then we can expect that

$$V_{2e}^{eff} = \frac{1}{2}V_{ds} \tag{12}$$

It is worth noting that, in order to test the validity of eq 12, V_{ds} can be estimated from the 4s admixture into the $3d(3z^2-r^2)$ level calculated for different Q_θ distortions. Indeed, the $|\phi_0(3z^2-r^2)\rangle$ orbital for $R_{eq} = R_{ax}$ becomes $|\widetilde{\phi(3z^2 - r^2)}\rangle$ when $Q_\theta \neq 0$, where

$$|\widetilde{\phi(3z^2 - r^2)}\rangle = |\phi_0(3z^2 - r^2)\rangle + \mu(Q_\theta)|\phi_0(4s)\rangle \tag{13}$$

$$\mu(Q_\theta) \cong -\frac{\langle\phi_0(3z^2 - r^2)|W_{1\theta}(\mathbf{r})|\phi_0(4s)\rangle}{\Delta_{ds}}Q_\theta \tag{14}$$

Of course, $|\phi_0(4s)\rangle$ is *not a pure* 4s wave function of nickel but involves admixtures of orbitals belonging to ligand ions. For simplicity, let us write

$$|\phi_0(4s)\rangle = \alpha_s|4s\rangle - \beta_s|\chi\rangle \tag{15}$$

Here ${\alpha_s}^2$ reflects the 4s admixture in $|\phi_0(4s)\rangle$, while the second term shortly describes the other contributions. In the calculations, it is relatively easy to determine the amount, $f_{4s}(Q_\theta)$, of $|4s\rangle$ in $|\widetilde{\phi(3z^2 - r^2)}\rangle$, which, according to eqs 13−15, is just given by

$$f_{4s}(Q_\theta) \equiv \mu(Q_\theta)^2{\alpha_s}^2 \tag{16}$$

Therefore, V_{ds} can be estimated from the calculated $f_{4s}(Q_\theta)$ curve and the Δ_{ds} value through the expression

$$V_{ds} = -\left[\frac{f_{4s}(Q_\theta)}{{Q_\theta}^2{\alpha_s}^2}\right]\Delta_{ds} \tag{17}$$

Because the results obtained on NaCl:Ni^+ are compared with those[11,13,36] for NaCl:Rh^{2+} where there is only one unpaired electron in the e_g shell, the corresponding expressions for $E(A_{1g})$ and $E(B_{1g})$ are

$$E(A_{1g}) = -V_{1e}Q_\theta + V_{2a}{Q_\theta}^2 + V_{3a}{Q_\theta}^3 + [V_{2e} + V_{ds}]{Q_\theta}^2 + \ldots \tag{18}$$

$$E(B_{1g}) = V_{1e}Q_\theta + V_{2a}{Q_\theta}^2 + V_{3a}{Q_\theta}^3 + V_{2e}{Q_\theta}^2 + \ldots \tag{19}$$

Thus if V_{3a} and V_{ds} are both negative, they favor an elongated geometry for NaCl:Rh^{2+}, where the unpaired electron is placed in the ${a_{1g}}^*(\sim 3z^2-r^2)$ orbital. This situation has been well observed experimentally.[18]

4. RESULTS AND DISCUSSION

In a first step, we have calculated the equilibrium Ni^+-Cl^- distance, R_{oct}, for the *average* $(3z^2 - r^2)^{1.5}(x^2 - y^2)^{1.5}$ configuration.[58,11] Because in this configuration the two orbitals are equally populated, there is no JT effect like happens for the ground state of Ni^{2+} in octahedral coordination. All performed calculations using different methods, functionals, and basis sets lead to similar results. For example, the value R_{oct} = 2.69 Å derived using a 87-ion cluster, the GGA-BP86 functional,[53,54] and relaxing only the ligand shell is found to be only 1 pm smaller than that coming from a 64-ion supercell calculation and the hybrid B1WC functional.[46] This result points out that the $Na^+ \rightarrow Ni^+$ substitution induces a small inward relaxation of 4% and suggests an ionic radius of 0.90 Å for Ni^+. This figure is thus consistent with a previous estimation.[59] Additional calculations on a 87-atom cluster have been performed where the distance R(Ni−Na) between the impurity and closest Na^+ ion along ⟨100⟩ directions has also been taken as variable in the minimization procedure. The calculated equilibrium distance R(Ni−Na) = 5.59 Å is found to be only 1% smaller than the lattice parameter a = 5.64 Å. Thus, the mismatch due to the slightly different ionic radius of Na^+ and Ni^+ mainly affects the average Ni^+-Cl^- distance.

In a second step, we have been working with the real $(3z^2 - r^2)^2(x^2 - y^2)^1$ (B_{1g} state) and $(3z^2 - r^2)^1(x^2 - y^2)^2$ (A_{1g} state) configurations, paying particular attention to obtaining the equilibrium geometry for the elongated and compressed conformations and also the corresponding energy difference, B. For clarifying this matter, a considerable number of periodic and cluster calculations have been performed by varying the basis set, the employed functional, and the cluster size. As a salient feature, we have found that in *all* performed calculations the $|B|$ value for NaCl:Ni^+ is *less* than 160 cm^{-1}, thus certainly smaller than the values derived for NaCl:Rh^{2+} (B = 511 cm^{-1}),[11,13] NaCl:Ag^{2+} (B = 500 cm^{-1}), or KCl:Ag^{2+} (B = 1024 cm^{-1}).[35]

Values of the equilibrium R_{eq} and R_{ax} distances for both the B_{1g} and A_{1g} states and the barrier B derived through *representative* periodic supercell and cluster calculations are gathered in Tables 1 and 2, respectively. In the case of periodic calculations, most of the values obtained with the best basis set give rise to positive B values in the range 80−120 cm^{-1}. We have verified that when the quality of the basis set is reduced, negative B values are more frequently encountered.

A similar picture emerges when looking at cluster calculations. Interestingly, the obtained value of B is found to be little dependent on the cluster size, and so in the clusters containing 39, 87, and 123 atoms, the value of B is always lying in the range 70−96 cm^{-1}, keeping the same functional and basis set (Table 2). As happens in the case of periodic calculations, a change of the functional can lead to the appearance of negative B values although $|B|$ is found to be always smaller than 160 cm^{-1}. In particular, this situation is found using the B3LYP functional in a spin-unrestricted calculation such as is shown in Table 2. It is worth noting that because $|B|$ is small it is not surprising that some calculations yield negative B values. A similar situation is encountered for CaO:Ag^{2+}, where experimental results[60] are consistent with a static JT effect and an elongated equilibrium geometry while ab initio calculations[61,13] gave B = −135 cm^{-1}.

dx.doi.org/10.1021/ic4009009 | Inorg. Chem. 2013, 52, 9338−9348

Table 1. Results of Periodic Supercell Calculations for the NaCl:Ni$^+$ Center in the B_{1g} and A_{1g} States, Using Different Functionals and Basis Sets[a]

basis set	functional	state	R_{eq}	R_{ax}	Q_θ	B
GTO	hybrid PW1PW	B_{1g}	2.560	2.845	0.329	+120
		A_{1g}	2.723	2.529	−0.224	
GTO	hybrid B1WC	B_{1g}	2.523	2.828	0.352	+80
		A_{1g}	2.679	2.497	−0.210	
GTO	LDA	B_{1g}	2.487	2.784	0.343	+112
		A_{1g}	2.625	2.454	−0.197	
GTO	GGA-PBEsol	B_{1g}	2.512	2.811	0.345	−160
		A_{1g}	2.667	2.460	−0.240	
PW	GGA-PBE	B_{1g}	2.503	2.886	0.442	+8
		A_{1g}	2.730	2.458	−0.314	

[a]Here GTO corresponds to the recently published pob-TZVP-2012 Gaussian basis set[38] for the *CRYSTAL* code, while PW means a plane-wave basis set in the *Quantum-Espresso* code.[50] R_{eq} and R_{ax} are the equilibrium equatorial and axial Ni$^+$−Cl$^-$ distances (in Å) and B is the energy barrier (in cm^{-1}) between the A_{1g} and B_{1g} states. Values of the Q_θ coordinate at equilibrium (in Å) are also reported.

Table 2. Representative Values of the Equilibrium R_{eq} and R_{ax} Distances (in Å) for Both the B_{1g} and A_{1g} States and the Energy Barrier, B (in cm^{-1}), for NaCl:Ni$^+$ Calculated by Means of Clusters of 39, 87, and 123 Atoms[a]

size	functional	state	R_{eq}	R_{ax}	Q_θ	B
39	GGA-BP86	B_{1g}	2.562	2.901	0.391	+96
		A_{1g}	2.783	2.491	−0.34	
87	GGA-BP86	B_{1g}	2.575	2.858	0.327	+74
		A_{1g}	2.767	2.497	−0.312	
123	GGA-BP86	B_{1g}	2.563	2.873	0.358	+88
		A_{1g}	2.767	2.483	−0.327	
87	GGA-PBE	B_{1g}	2.589	2.870	0.324	+55
		A_{1g}	2.772	2.526	−0.28	
87	B3LYP	B_{1g}	2.648	2.861	0.25	−140
		A_{1g}	2.797	2.595	−0.23	

[a]These results have been obtained using the BP86 functional[53,54] and also the PBE[51] and B3LYP[55] functionals. The value of the Q_θ coordinate at equilibrium (in Å) is also reported.

As to the experimental **g** tensor of NaCl:Ni$^+$ at T = 20 K, the values $g_\parallel$ = 2.86 and $g_\perp$ = 2.10 prove[15] that the unpaired electron is placed in the $b_{1g}^*(\sim x^2-y^2)$ orbital and thus B is positive.

With regard to the equilibrium R_{eq} and R_{ax} values calculated for both the B_{1g} and A_{1g} states using different procedures (Tables 1 and 2), it can be seen that there is a reasonable agreement among them. Nevertheless, variation of the calculated R_{eq} and R_{ax} values reported on Tables 1 and 2 shows differences up to 4%. For comparison, cluster and periodic supercell calculations on MgO:Cr^{3+} using different types of functionals and changing the number of involved ions all lead[56] to the same value of the Cr^{3+}−O^{2-} distance within 0.8%. This underlines the difficulties for studying the Ni$^+$ impurity in comparison with Cr^{3+}, where the 3d−4s separation amounts[19] to 14 eV.

Let us now focus on the calculated values of d−d transitions for NaCl:Ni$^+$ at the corresponding equilibrium geometry. The results for the $a_{1g}^*(\sim 3z^2-r^2) \rightarrow b_{1g}^*(\sim x^2-y^2)$, $b_{2g}^*(\sim xy) \rightarrow b_{1g}^*$, and $e_g^*(\sim xz;yz) \rightarrow b_{1g}^*$ transition energies (called Δ_0, Δ_1, and Δ_2, respectively) are collected in Table 3 together with the energy for the first allowed charge-transfer transition $e_u(\pi) \rightarrow b_{1g}^*$. Such figures are compared with experimental values measured[62−64,35] for CdCl$_2$:Cu^{2+} and KCl:Ag^{2+}. It can be noticed that Δ_0, Δ_1, and Δ_2 values are much smaller for NaCl:Ni$^+$ than for other *divalent* 3d^9 and 4d^9 cations, stressing the singularity of the monovalent Ni$^+$ ion. For instance, the calculated Δ_1 value for NiCl$_6^{5-}$ in NaCl is around *one-third* that measured[62] for the CuCl$_6^{4-}$ complex in CdCl$_2$, pointing out that 10Dq decreases upon passing from trivalent to divalent impurities[65] and especially from the last ones to monovalent cations. Along this line, a value Δ_1 = 4700 cm^{-1} was estimated[34] for AgCl:Ni$^+$.

Table 3. Values of the Three d−d Transition Energies and the $e_u(\pi) \rightarrow b_{1g}^*$ Charge-Transfer Transition Energy for NaCl:Ni$^+$ Calculated at the Ground-State Equilibrium Geometry[a]

	Δ_0	Δ_1	Δ_2	$e_u(\pi) \rightarrow b_{1g}^*$
NaCl:Ni$^+$ (BP86)	1806	3725	3975	56445
NaCl:Ni$^+$ (PW1PW)	*1530*	*3300*	*3470*	*71000*
CdCl$_2$:Cu^{2+}	6372	9437	10970	25510
KCl:Ag^{2+}	12500	15900	17820	21700

[a]Δ_0, Δ_1, and Δ_2 mean the energies of the transitions from respectively $a_{1g}^*(\sim 3z^2-r^2)$, $b_{2g}^*(\sim xy)$, and $e_g^*(\sim xz;yz)$ antibonding orbitals to the $b_{1g}^*(\sim x^2-y^2)$ one. The results obtained for DFT cluster calculations on NaCl:Ni$^+$ using BP86 (R_{eq} = 2.563 Å; R_{ax} = 2.873 Å) and PW1PW (R_{eq} = 2.560 Å; R_{ax} = 2.845 Å) functionals are both reported and compared to experimental values for D_{4h} CuCl$_6^{4-}$[62−64,63] and AgCl$_6^{4-}$ complexes.[64] All energies are in cm^{-1} units.

Although no optical measurements on the d−d transitions of Ni$^+$ impurities in insulators have hitherto been reported, the results collected in Table 3 are qualitatively consistent with the high $g_\parallel - g_0$ = 0.86 value measured[15] for NaCl:Ni$^+$ compared with $g_\parallel - g_0$ = 0.34 derived[66] for CdCl$_2$:Cu^{2+} because $g_\parallel - g_0$ depends in second-order perturbation[67,68] on $(\Delta_1)^{-1}$. Furthermore, using the general expressions for $g_\parallel - g_0$ and $g_\perp - g_0$ given in ref 68, the geometry optimized in the periodic PW1PW calculations, the Δ_1 and Δ_2 values of Table 3, and the covalency coefficients also derived from the present calculations, we have found $g_\parallel - g_0$ = 0.89 and $g_\perp - g_0$ = 0.16. Such values are thus not far from the experimental figures.[15] With regard to the covalency, if we simply write the normalized wave function of the antibonding $b_{1g}^*(\sim x^2-y^2)$ orbital as

$$|b_{1g}^*(x^2-y^2)\rangle = \alpha|3d(x^2-y^2)\rangle - \beta|\chi_L\rangle \qquad (20)$$

we have found α^2 = 0.90 for NiCl$_6^{5-}$ in NaCl, thus pointing out that the unpaired electron is essentially residing on the central cation, while a higher covalency is obtained[68] for CuCl$_6^{4-}$ (α^2 = 0.70) and especially for AgCl$_6^{4-}$ where α^2 = 0.50.[69] In eq 20, $|\chi_L\rangle$ shortly denotes a linear combination of 3p and 3s orbitals of equatorial Cl$^-$ ligands. The increase of covalency upon passing from NiCl$_6^{5-}$ to AgCl$_6^{4-}$ is qualitatively consistent with the significant decrease of the energy of the first allowed charge-transfer transition $e_u(\pi) \rightarrow b_{1g}^*$ (Table 3). Accordingly, the optical electronegativity,[70,28,71] x_{opt}, of Ni$^+$ should be around 1.1. The singularity of the monovalent Ni$^+$ ion is obvious when comparing this value with the empirical values estimated by Jørgensen[70] for Ni^{2+} and Cu^{2+}, x_{opt} = 2.2 and 2.4, respectively, or the obtained[69,72] for Ag^{2+} and Rh^{2+}, x_{opt} = 2.8 and 2.5, respectively.

Concerning the barrier, B, a rough estimation of this quantity for NaCl:Ni$^+$ can be obtained from temperature T_t = 35 K at which the static spectrum starts to disappear[15] in conjunction

dx.doi.org/10.1021/ic4009009 | *Inorg. Chem.* 2013, 52, 9338−9348

with the calculated value[35] $B = 500$ cm^{-1} for NaCl:Ag^{2+} and the corresponding experimental value[16] $T_t = 95$ K also measured in X-band EPR experiments. Let us denote by ν the jump frequency between two equivalent minima separated by the barrier B. Assuming an Arrhenius type law for the temperature dependence of ν, it can be written as

$$\nu = \nu_0 e^{-B/kT} \tag{21}$$

The transition between a static EPR spectrum and an average isotropic one requires that[9,35]

$$h\nu \approx (g_{\parallel} - g_{\perp})\beta H \tag{22}$$

where β denotes the Bohr magneton. Then, because $H \approx 300$ mT (X band) and $g_{\parallel} - g_{\perp} = 0.155$ for NaCl:Ag^{2+},[16] if we assume that the ratio ν_0(NaCl:Ag^{2+})/ν_0(NaCl:Ni^{+}) lies roughly between 1 and 2, we get B(NaCl:Ni^{+}) ≈ 120 cm^{-1}. Thus, the positive B values obtained in periodic and cluster calculations (Tables 1 and 2) are compatible with this estimation.

A central matter in this research is to understand why the B value for NaCl:Ni^{+} is much smaller than those derived for Ag^{2+}-doped NaCl and KCl[35] and for NaCl:Rh^{2+}.[11,13] To achieve this goal, we have analyzed the results derived for NaCl:Ni^{+} with a 87-ion cluster (Figure 3), giving $B = 74$ cm^{-1} (Table 2), by means of the procedure explained in section 3.[11] It is worth noting that the value $Q_\theta = 0.327$ Å derived for the elongated conformation of NaCl:Ni^{+} (Table 2) is practically coincident with $Q_\theta = 0.320$ Å obtained[11,13,36] for NaCl:Rh^{2+}. This implies that knowledge of the magnitude of the distortion alone does not allow prediction of the value of B.

Seeking to clear out this matter, the calculated $E(A_{1g};Q_\theta)$ and $E(B_{1g};Q_\theta)$ curves, displayed in Figure 4, have been explored

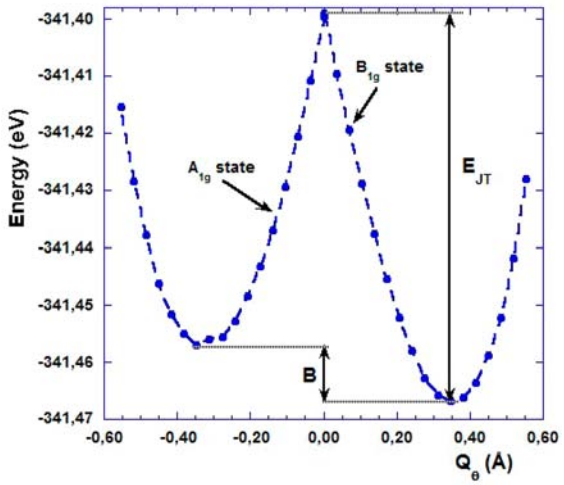

Figure 4. Picture of the calculated total energy as a function of the Q_θ coordinate for B_{1g} and A_{1g} electronic states of NaCl:Ni^{+}. The results shown here have been derived through a calculation on the 87 ions cluster using the BP86 functional.[53,54]

through the procedure explained in section 3.[11] From the calculated $[E(A_{1g}) + E(B_{1g})]/2$ and $[E(A_{1g}) - E(B_{1g})]/2$ quantities, the values of V_{1e}, V_{2a}, V_{3a}, and V_{2e}^{eff} have been determined. The main results obtained for NaCl:Ni^{+} are collected in Table 4, where they are compared to those[11,13,36,52] for NaCl:Rh^{2+}. It can be noticed that while for NaCl:Rh^{2+} the curvature at the minimum of the compressed geometry is

Table 4. Values of V_{1e}, V_{2a}, V_{3a}, and V_{2e}^{eff} Vibronic Constants (in eV/Å, eV/Å^2, eV/Å^3, and eV/Å^2, Respectively) and the Barrier, B (in cm^{-1}), Derived for NaCl:Ni^{+} from the Calculation of the 87-Atom Cluster with the GGA-BP86 Functional[a]

system	V_{1e}	V_{2a}	V_{3a}	V_{2e}^{eff}	E_{JT} (cm^{-1})	B (cm^{-1})
NaCl:Ni^{+}	0.32	0.90	0.26	−0.16	534	72
NaCl:Rh^{2+}	1.40	2.8	−1.1	−0.21	1830	511

[a]Such data are compared to those previously obtained[11,13] for NaCl:Rh^{2+}. The value of the JT energy, E_{JT}, obtained for NaCl:Ni^{+} is also given and compared to that recently found for NaCl:Rh^{2+} by two different groups.[13,36].

clearly higher than that for the elongated conformation,[58] this is not true for NaCl:Ni^{+}.

With regard to calculated values, $V_{1e} = 0.32$ eV/Å derived for NaCl:Ni^{+} is about 4 times smaller than $V_{1e} = 1.40$ eV/Å previously derived[11] for NaCl:Rh^{2+} (Table 4). This reduction is qualitatively consistent with that experienced by 10Dq upon passing from divalent cations to a monovalent cation like Ni^{+}. On the other hand, the value $V_{1e} = 0.32$ eV/Å is essentially compatible with the figure $\Delta_0 = 1530$ cm^{-1} given in Table 3 and $Q_\theta = 0.327$ Å because in a first approximation[11,12]

$$\Delta_0 = 2V_{1e}Q_\theta \tag{23}$$

It is worth noting that while in comparison to NaCl:Rh^{2+} the values of V_{2a} and $|V_{3a}|$ obtained for NaCl:Ni^{+} are significantly reduced, this is not the case for the V_{2e}^{eff} quantity. As the obtained value for NaCl:Ni^{+}, $V_{2e}^{eff} = -0.16$ eV/Å^2, is negative, this is qualitatively consistent with the assumption that $V_{2e}^{eff} = V_{ds}/2$ mainly arises from the 3d($3z^2-r^2$)−4s vibronic coupling because, according to eq 6, $V_{ds} < 0$. Moreover, the term involving V_{ds} in eq 12 gives rise to a barrier $B = 240$ cm^{-1}.

As a salient feature, the sign of the anharmonic coefficient, $V_{3a} = 0.26$ eV/Å^3, is found to be *positive* for NaCl:Ni^{+}, a result that is thus completely at variance with what is found for NaCl:Rh^{2+}, where[11] $V_{3a} = -1.1$ eV/Å^3. This relevant result just means that the equilibrium geometry for NaCl:Ni^{+} would be compressed if *only* the anharmonic contribution is taken into account. More precisely, with the Q_θ values given in Table 2, the contribution to the barrier from the $V_{3a}(\rho_C^3 + \rho_E^3)$ term in eq 12 is equal to -135 cm^{-1}, while that coming from the first two terms involving the V_{1e} and V_{2a} coefficients is equal only to -24 cm^{-1}. These results thus point out that the elongated geometry of the $NiCl_6^{5-}$ complex in NaCl:Ni^{+} is mainly due to the 3d($3z^2-r^2$)−4s vibronic coupling, although its contribution to B is canceled to an important extent by that arising from the anharmonicity. This explains albeit qualitatively the low value of B for NaCl:Ni^{+} in comparison with those obtained[11,13,35] for NaCl:Rh^{2+}, NaCl:Ag^{2+}, and KCl:Ag^{2+}.

Seeking to test the reliability of the $V_{2e}^{eff} = V_{ds}/2$ assumption, we have estimated V_{ds} by means of eqs 16 and 18. From our calculations, we have determined the amount, $f_{4s}(Q_\theta)$, of |4s⟩ admixture into $|\phi(\widetilde{3z^2 - r^2})\rangle$. The results in Figure 5 show that $f_{4s}(Q_\theta)$ is actually proportional to Q_θ^2 with $f_{4s}(Q_\theta)/Q_\theta^2 = 0.085$ Å^{-2}. On the other hand, the |4s⟩ admixture in $|\phi_0(4s)\rangle$ is found to be $\alpha_s^2 = 0.70$, while the present calculations give $\Delta_{ds} = 2.5$ eV. Therefore, according to eqs 16 and 18, we estimate $V_{ds} = -0.30$ eV/Å^2 and thus $V_{ds}/2$ is close to the value $V_{2e}^{eff} = -0.15$ eV/Å^2 derived from analysis of the results collected in Table 3. This analysis thus strongly supports that the elongated

dx.doi.org/10.1021/ic4009009 | Inorg. Chem. 2013, 52, 9338−9348

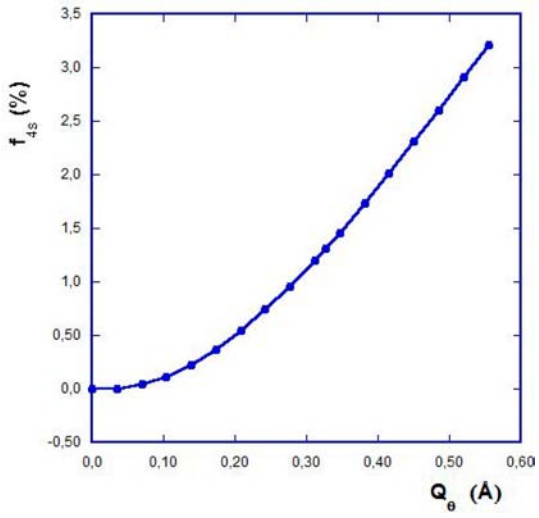

Figure 5. Calculated values of f_{4s} as a function of the Q_θ coordinate. The f_{4s} quantity reflects the amount of |4s⟩ wave function found in the $a_{1g}^*(\sim 3z^2-r^2)$ orbital.

geometry obtained for NaCl:Ni^+ is mainly due to the $3d(3z^2-r^2)-4s$ vibronic coupling.

A central point in the present analysis is to understand why the *sign* of the anharmonic parameter, V_{3a}, is found to be *positive* in NaCl:Ni^+, while it is clearly negative for NaCl:Rh^{2+}. As has been pointed out before, in NaCl:Rh^{2+} the $RhCl_6^{4-}$ complex is practically *elastically decoupled* from the rest of the lattice,[61,21] while this situation is likely not to be true for NaCl:Ni^+, where Ni^+ and Na^+ are both monovalent ions. A simple model[61,21] for clarifying the two different situations is depicted in Figure 6. In such a figure, a given ligand, X, is *attached* to the impurity ion, M, as well as to the closest A host lattice cation along a ⟨100⟩ direction. Let us now consider the motion of the ligands only along the M−X directions, keeping M and A *fixed*. In such a case, when a ligand is not in its equilibrium position, there are two springs that are activated. If we consider, in principle, a single M−X−A unit, then the associated potential energy can be described by

$$U_p(\mathrm{M-X-A}) = \frac{1}{2}k(u_X)^2 + \frac{1}{2}k'(u_X)^2 - g(u_X)^3 + g'(u_X)^3 \quad (24)$$

In this expression, u_X describes the separation of the ligand coordinate along a ⟨100⟩ direction from its equilibrium position. If $u_X > 0$, it means that the ligand is moving away from the impurity and thus *approaching* the A ion. If we assume that the anharmonicity in *both* the M−X and X−A bonds favors the elongation of both springs, then g and g' must be positive. It should be recalled that in a simple diatomic molecule $g > 0$ is actually responsible for a positive thermal expansion coefficient. For this reason, the *total* anharmonic energy of the M−X−A unit favors a compressed situation in the M−X bond, *provided* that $g' > g$. Let us now consider a Q_θ distortion involving the six ligands. Because the anharmonic energy of a single M−X−A unit is equal to $(g' - g)u_X^3$, V_{3a} is simply given by

$$V_{3a} = \frac{1}{\sqrt{12}}(g' - g) \quad (25)$$

When the complex is elastically decoupled from the rest of the lattice, this implies that $k \gg k'$ and $g \gg g'$ and then V_{3a} is necessarily negative, pointing out that an elongation described by Q_θ yields a smaller energy increase than a $-Q_\theta$ compression. By contrast, in a case like NaCl:Ni^+, where both monovalent ions have a similar ionic radius, the conditions $k \gg k'$ and $g \gg g'$ are not necessarily fulfilled.

Seeking to clear out this relevant matter we have estimated from the present calculations the values of the two constants k and k' in eq 21. While $k'/k = 0.28$ for NaCl:Rh^{2+},[61] a much higher value $k'/k = 2.9$ has been obtained for NaCl:Ni^+. This result strongly supports that in the last case the $NiCl_6^{5-}$ complex is *elastically coupled* to the rest of the lattice and thus it can reasonably be expected that $g' > g$. This reasoning thus explains why V_{3a} is negative for NaCl:Rh^{2+} while it can be positive for the present case.

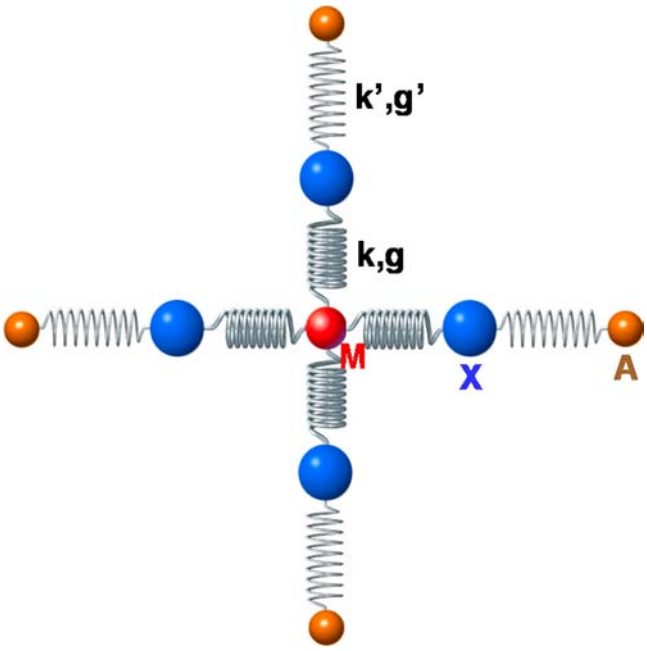

Figure 6. Model system for discussing the anharmonic energy of a Q_θ distortion. The ligands move along ⟨100⟩ directions, while the A and M atoms are fixed.

5. FINAL REMARKS

According to the present results, the understanding of the actual geometry displayed by a seemingly simple JT system is certainly a nontrivial problem requiring a detailed quantitative study. Indeed, it has been shown that for NaCl:Ni^+ the two main contributions to the barrier have an *opposite* sign and thus the calculated $|B|$ value is certainly smaller than $B \approx 500$ cm^{-1} obtained for NaCl:M^{2+} (M = Rh, Ag) and $B = 1024$ cm^{-1} derived[11,13,35] for KCl:Ag^{2+}. Because of this special situation, it is not surprising to find that some calculations on NaCl:Ni^+ lead to negative B values, although $|B|$ is always smaller than 160 cm^{-1}.

As a salient feature, the present study supports that the equilibrium elongated geometry observed experimentally for $NiCl_6^{5-}$ in NaCl is mainly due to the $3d(3z^2-r^2)-4s$ vibronic mixing. To our knowledge, NaCl:Ni^+ is the first JT system in which it has quantitatively been demonstrated that the *dominant* contribution to the barrier arises from such a vibronic mixing. This result thus stresses that the barrier in JT systems cannot be understood at all, neglecting the changes of the electronic density accompanying the small distortions.

dx.doi.org/10.1021/ic4009009 | Inorg. Chem. 2013, 52, 9338−9348

The present results for NaCl:Ni^+ are thus fully different from those found for NaCl:Rh^{2+}[11] or KCl:Ag^{2+},[35] where the barrier comes mainly from the anharmonicity. Therefore, in NaCl:Ni^+ the electronic structure of the impurity plays a key role for understanding the equilibrium geometry. Indeed, in the case of *free* ions, the nd−(n+1)s separation is equal[19] to 2 eV for Ni^+ (n = 3), 8 eV for Cu^{2+} (n = 3), 9 eV for Rh^{2+} (n = 4), 9 eV for Ag^{2+} (n = 4), and 14 eV for Cr^{3+} (n = 3).

It is worth noting that EPR data prove that in K_2MgF_4:Ni^+ the local geometry of NiF_6^{5-} corresponds to an elongated octahedron,[73] while in K_2ZnF_4:Cu^{2+}, CuF_6^{4-} is, however, compressed.[74,22] Again the small 3d−4s separation in Ni^+ has been shown to play a key role for explaining this surprising situation.[75]

The present analysis supports that in NaCl:Ni^+ the anharmonicity of the e_g mode alone favors a compressed rather than an elongated geometry. This fact just reflects that the $NiCl_6^{5-}$ complex is not elastically decoupled from the rest of the lattice like when Na^+ is replaced by a smaller divalent cation. This situation is thus quite different from that of *free* molecules subject to the JT effect as discussed in refs 76 and 77.

Although EPR work carried out on $KMgF_3$:Ni^+[31] or $CsCaF_3$:Ni^+[32] proves that the JT center formed in these systems exhibits an elongated geometry, it has been assumed by several authors that in LiF:Ni^+ and NaF:Ni^+ such a center displays a compressed geometry.[29,67,78,79] Nevertheless, there are serious arguments against the correctness of this assignment as discussed in refs 80 and 81.

Because of the low values of the barrier in NaCl:Ni^+, it is interesting to explore why coherent tunneling is not observed instead of a static JT effect. When coherent tunneling among equivalent distortions takes place, the EPR spectrum exhibits a cubic rather than a tetragonal pattern, a situation termed the dynamic JT effect.[9−14] The unavoidable presence of random strains in any real crystal very often destroys the coherence,[9] and then an EPR spectrum characteristic of a static JT effect with D_{4h} symmetry is usually observed for d^9 ions in cubic halides.[10] Calling δ_s the energy splitting induced by a tetragonal random strain on the vibronic doublet, the occurrence of a dynamic JT effect requires that $3\Gamma > \delta_s$, where 3Γ is the tunneling splitting[9,13,14] and δ_s is thus a *sample-dependent* quantity. Because up to now no direct measurement of 3Γ has been performed for MgO:Cu^{2+}, where a dynamic JT effect has been observed experimentally,[82] the situation on the actual value of 3Γ and the ratio $\delta_s/3\Gamma$ is still controversial. In this sense, Reynolds et al. obtained[82] a ratio $\delta_s/3\Gamma$ = 0.1 from analysis of the available EPR data, while more recently Riley et al.[83] give $\delta_s/3\Gamma$ = 0.5. On the other hand, ab initio results on MgO:Cu^{2+} give[13,14] 3Γ = 235 cm^{-1}, while the calculated 3Γ value[13,14] for the two other cases[60,82] (MgO:Ag^{2+} and CaO:Cu^{2+}), where a dynamic JT effect has actually been observed, is always *higher than* 50 cm^{-1}. Furthermore, a theoretical study carried out on MgO:Cu^{2+} points out that the dynamic JT effect is already destroyed[14] when $\delta_s/3\Gamma > 0.2$. This standpoint is consistent with the observation[60] of a *static* JT effect in CaO:Ag^{2+}, where the calculated 3Γ value[13,14] is equal to 30 cm^{-1}.

With regard to NaCl:Ni^+, the calculated kinetic energy for the vibronic ground state[13,14] when B = 0, E_k, is equal to $\hbar^2/8M_X\rho_E^2$ = 1.2 cm^{-1}, which is certainly smaller than the actual value of the barrier B. Here M_X is the ligand mass and ρ_E corresponds to the equilibrium Q_θ value for the B_{1g} state.[13,14] For this reason, it can reasonably be expected that the actual 3Γ for NaCl:Ni^+ will be clearly smaller than $3\Gamma = 8E_k$ = 9 cm^{-1} calculated[13,14] when there is no barrier at all. Thus, the present analysis and the typical values[14] of δ_s (∼10 cm^{-1}) strongly favor the observation of a static JT effect in NaCl:Ni^+ in agreement with the experimental data.[15]

The present results stress the importance of ab initio calculations for reaching a microscopic understanding of mechanisms responsible for the observed equilibrium geometry. In this sense, most of the experimental information on systems displaying a static JT effect corresponds to the electronic ground state. Therefore, although the usual EPR fingerprints[67] of elongated [$g_\parallel - g_0 \approx 4(g_\perp - g_0)$] and compressed ($g_\perp - g_0 > 0$ and $g_\parallel - g_0 \approx 0$) conformations for d^9 impurities are very different, it is not easy to know the *small* energy difference between them only from the experimental data. On the other hand, calculations provide insight into the parameters involved in the usual *effective* JT Hamiltonians, thus avoiding unnecessary speculations in the models.

In conclusion, analysis of the ab initio calculations in JT systems provides very crucial information on the subtle origin of the equilibrium geometry. Further work along this line is now underway.

■ ASSOCIATED CONTENT

Supporting Information

More details on the cluster calculations, as well as the optimized geometries. This material is available free of charge via the Internet at http://pubs.acs.org.

■ AUTHOR INFORMATION

Corresponding Author

*E-mail: barriust@unican.es.

Notes

The authors declare no competing financial interest.

■ ACKNOWLEDGMENTS

Support by the Spanish Ministerio de Ciencia y Tecnología under Projects FIS2012-30996 and FIS2009-07083 is acknowledged. J.M.G.L. acknowledges support from the Spanish Ministry of Economy and Competitiveness under Project FIS2010-21282-C02-01 and through Ramon y Cajal grant RYC-2011-07782.

■ REFERENCES

(1) Babel, D.; Tressaud, A. In *Inorganic Solid Fluorides*; Hagenmuller, P., Ed.; Academic Press: New York, 1985.

(2) Garcia-Fernandez, P.; Aramburu, J. A.; Barriuso, M. T.; Moreno, M. *J. Phys. Chem. Lett.* **2010**, *1*, 647−651.

(3) Spaeth, J. M.; Koschnick, F. *J. Phys. Chem. Solids* **1991**, *52*, 1−34.

(4) Breñosa, A. G.; Moreno, M.; Rodriguez, F.; Couzi, M. *Phys. Rev. B* **1991**, *44*, 9859−9863.

(5) Riley, M.; Hitchman, M. A.; Reinen, D.; Steffen, G. *Inorg. Chem.* **1988**, *27*, 1924−1934.

(6) Garcia-Fernandez, P.; García-Lastra, J. M.; Trueba, A.; Barriuso, M. T.; Aramburu, J. A.; Moreno, M. *Phys. Rev. B* **2012**, *85*, 094110-1−094110-9.

(7) Hauser, A.; Enachescu, C.; Daku, M. L.; Vargas, A.; Amstutz, N. *Coord. Chem. Rev.* **2006**, *250*, 1642−1652.

(8) Venkataramani, S.; Jana, U.; Dommaschk, M.; Sönnichsen, F. D.; Tuczek, F.; Herges, R. *Science* **2011**, *331*, 445−448.

(9) Ham, F. S. In *Electron Paramagnetic Resonance*; Geschwind, S., Ed.; Plenum: New York, 1972.

(10) Bill, H. In *The Dynamical Jahn–Teller Effect in Localized Systems*; Perlin, Yu. E., Wagner, M., Eds.; Elsevier: Amsterdam, The Netherlands, 1984.
(11) García-Fernández, P.; Bersuker, I. B.; Aramburu, J. A.; Barriuso, M. T.; Moreno, M. *Phys. Rev. B* **2005**, *71*, 184117–1–10.
(12) Bersuker, I. B. *The Jahn–Teller effect*; Cambridge University Press: Cambridge, U.K., 2006.
(13) Garcia-Fernandez, P.; Trueba, A.; Barriuso, M. T.; Aramburu, J. A.; Moreno, M. *Phys. Rev. Lett.* **2010**, *104*, 035901–1–4.
(14) Garcia-Fernandez, P.; Trueba, A.; Barriuso, M. T.; Aramburu, J. A.; Moreno, M. *Vibronic Interactions and the Jahn–Teller Effect*; Daul, C., Atanasov, M., Tregenna-Piggott, P. L. W., Eds.; Springer-Verlag: Heidelberg, Germany, 2012; p 105.
(15) Shengelaya, A.; Drulis, H.; Macalik, B.; Suzynska, M. *Z. Phys. B* **1996**, *101*, 373–376.
(16) Sierro, J. *J. Phys. Chem. Solids* **1967**, *28*, 417–422.
(17) Borchert, R. H.; Kanzaki, H.; Abe, H. *Phys. Rev. B* **1970**, *2*, 23–27.
(18) Vercammen, H.; Schoemaker, D.; Briat, B.; Ramaz, F.; Callens, F. *Phys. Rev. B* **1999**, *59*, 286–292.
(19) Moore, C. E. *Atomic Energy Levels*; Nat. Stand. Ref. Pat. Ser. Nat. Bur. Stand.: Washington, DC, 1971.
(20) Öpik, U.; Pryce, M. H. M. *Proc. R. Soc. London, Ser. A* **1957**, *238*, 425–447.
(21) Moreno, M.; Barriuso, M. T.; Aramburu, J. A.; Garcia-Fernandez, P.; Garcia-Lastra, J. M. *J. Phys.: Condens. Matter* **2006**, *18*, R315–R360.
(22) Reinen, D.; Atanasov, M. *Magn. Reson. Rev.* **1991**, *15*, 167–239.
(23) Reinen, D. *Inorg. Chem.* **2012**, *51*, 4458–4472.
(24) Yamatera, H. *Acta Chem. Scand.* **1979**, *A33*, 107–111.
(25) Gerloch, M. *Inorg. Chem.* **2012**, *20*, 638–640.
(26) Ceulemans, A.; Beyens, D.; Vanquickerborne, L. G. *Inorg. Chem. Acta* **1982**, *61*, 199–206.
(27) Deeth, R. J.; Hitchman, M. A. *Inorg. Chem.* **1986**, *25*, 1225–1233.
(28) Reinen, D.; Atanasov, M.; Kohler, P.; Babel, D. *Coord. Chem. Rev* **2010**, 2703–2754.
(29) Hayes, W.; Wilkens, J. *Proc. R. Soc. London, Ser. A* **1964**, *281*, 340–361.
(30) Rousseau, J. J.; Binois, M.; Fayet, J. C. *C. R. Acad. Sci. Paris* **1974**, *278*, 1079–1081.
(31) Zorita, E.; Alonso, P. J.; Alcala, R. *Phys. Rev. B* **1987**, *35*, 3116–3121.
(32) Villacampa, B.; Alcala, R.; Alonso, P. J.; Moreno, M.; Barriuso, M. T.; Aramburu, J. A. *Phys. Rev. B* **1994**, *49*, 1039–1047.
(33) Marchetti, A. P.; Scozzafava, M. *Phys. Status Solidi B* **1979**, *96*, 441–445.
(34) van Robbroeck, L.; Goovaerts, E.; Schoemaker, D. *Phys. Status Solidi B* **1985**, *132*, 179–187.
(35) Trueba, A.; Garcia-Lastra, J. M.; De Graaf, C.; Garcia-Fernandez, P.; Barriuso, M. T.; Aramburu, J. A.; Moreno, M. *Chem. Phys. Lett.* **2006**, *430*, 51–55.
(36) Sakhabutdinova, N.; van Yperen-De Deyne, A.; Pauwels, E.; van Speybroeck, V.; Vrielinck, H.; Callens, F.; Waroquier, M. *J. Phys. Chem. A* **2011**, *115*, 1721–1733.
(37) Dovesi, R.; Orlando, R.; Civalleri, B.; Roetti, C.; Saunders, V. R.; Zicovich-Wilson, C. M. *Z. Kristallogr.* **2005**, *220*, 571–573.
(38) Peintinger, M. F.; Vilela Oliveira, D.; Bredow, T. *J. Comput. Chem.* **2013**, *34*, 451–459.
(39) Freyria Fava, C. Laurea Thesis, Turin, 1995; p 93
(40) Dovesi, R.; Roetti, C.; Freyria Fava, C.; Prencipe, M.; Saunders, V. R. *Chem. Phys.* **1991**, *156*, 11–19.
(41) Apra, E.; Causá, M.; Prencipe, M.; Dovesi, R.; Saunders, V. R. *J. Phys.: Condens. Matter* **1993**, *5*, 2969–2976.
(42) CRYSTAL Basis Sets, http://www.crystal.unito.it/Basis_Sets/Ptable.html.
(43) Perdew, J. P.; Zunger, A. *Phys. Rev. B* **1981**, *23*, 5048–5079.
(44) Perdew, J. P.; Ruzsinszky, A.; Csonka, G. I.; Vydrov, O. A.; Scuseria, G. E.; Constantin, L. A.; Zhou, X.; Burke, K. *Phys. Rev. Lett.* **2008**, *100*, 136406-1–136406-4.
(45) Bilc, D. I.; Orlando, R.; Shaltaf, R.; Rignanese, G.-M.; Iñiguez, J.; Ghosez, Ph. *Phys. Rev. B* **2008**, *77*, 165107-1–165107-13.
(46) Bredow, T.; Gerson, A. *Phys. Rev. B* **2000**, *61*, 5194–5201.
(47) Urusov, V. S.; Blinov, V. V. *Izv. Akad. Nauk SSSR, Ser. Khim.* **1970**, *12*, 278–282.
(48) Poole, R. T.; Jenkin, J. G.; Liesegang, J.; Leckey, R. C. G. *Phys. Rev. B* **1975**, *11*, 5179–5189.
(49) García-Fernández, P.; Ghosh, S.; English, N. J.; Aramburu, J. A. *Phys. Rev. B* **2012**, *86*, 144107–1–12.
(50) Giannozzi, P.; et al. *J. Phys.: Condens. Matter* **2009**, *21*, 395502–1–19.
(51) Perdew, J. P.; Burke, K.; Ernzerhof, M. *Phys. Rev. Lett.* **1996**, *77*, 3865–3868.
(52) te Velde, G.; Bickelhaupt, F. M.; Baerends, E. J.; Guerra, C. F.; van Gisbergen, S. J. A.; Snijders, J. G.; Ziegler, T. *J. Comput. Chem.* **2001**, *22*, 931–967.
(53) Becke, A. D. *Phys. Rev. A* **1988**, *38*, 3098–3100.
(54) Perdew, J. P. *Phys. Rev. B* **1986**, *33*, 8822–8824.
(55) Becke, A. D. *J. Chem. Phys.* **1993**, *98*, 5648–5652.
(56) Aramburu, J. A.; Garcia-Fernandez, P.; García-Lastra, J. M.; Barriuso, M. T.; Moreno, M. *J. Phys.: Condens. Matter* **2013**, *25*, 175501-1–175501-8.
(57) Garcia-Fernandez, P.; Aramburu, J. A.; Barriuso, M. T.; Moreno, M. *J. Chem. Phys.* **2008**, *128*, 124513-1–124513-7.
(58) Barriuso, M. T.; Garcia-Fernandez, P.; Aramburu, J. A.; Moreno, M. *Solid State Commun.* **2001**, *120*, 1–5.
(59) Barriuso, M. T.; Moreno, M. *Solid State Commun.* **1984**, *51*, 335–338.
(60) Boatner, L. A.; Reynolds, R. W.; Abraham, M. M.; Chen, Y. *Phys. Rev. Lett.* **1973**, *31*, 7–10.
(61) Garcia-Fernandez, P.; Sousa, C.; Aramburu, J. A.; Barriuso, M. T.; Moreno, M. *Phys. Rev. B* **2005**, *72*, 155107-1–155107-5.
(62) Kan'no, K.; Mukai, S.; Nakai, Y. *J. Phys. Soc. Jpn.* **1974**, *36*, 1492–1492.
(63) Kan'no, K.; Naoe, S.; Mukai, S.; Nakai, Y.; Miyanaga, T. *Solid State Commun.* **1973**, *13*, 1325–1328.
(64) Delbecq, C. J.; Hayes, W.; O'Brien, M. C. M.; Yuster, P. H. *Proc. R. Soc. London, Ser. A* **1963**, *271*, 243–267.
(65) Barriuso, M. T.; Aramburu, J. A.; Moreno, M. *Phys. Status Solidi B* **1996**, *196*, 193–208.
(66) Hayashi, M.; Nakagawa, N.; Matsumoto, R. *Mem. Fac. Eng. Fukui Univ.* **1978**, *26*, 15–27.
(67) Abragam, A.; Bleaney, B. *Electron Paramagnetic Resonance of Transition Ions*; Clarendon: Oxford, U.K., 1970; p 464.
(68) Aramburu, J. A.; Moreno, M. *J. Chem. Phys.* **1985**, *83*, 6071–6083.
(69) Valiente, R.; Aramburu, J. A.; Barriuso, M. T.; Moreno, M. *J. Phys.: Condens. Matter* **1994**, *6*, 4515–4525.
(70) Jørgensen, C. K. *Prog. Inorg. Chem.* **1970**, *12*, 101–158.
(71) Moreno, M.; Aramburu, J. A.; Barriuso, M. T. *Struct. Bonding (Berlin)* **2004**, *106*, 127–152.
(72) Garcia-Fernandez, P.; Barriuso, M. T.; Aramburu, J. A.; Moreno, M. *Chem. Phys. Lett.* **2003**, *374*, 151–156.
(73) Alcalá, R.; Zorita, E.; Alonso, P. J. *J. Phys. C: Solid State Phys.* **1988**, *21*, 461–470.
(74) Hitchman, M. A.; McDonald, R. G.; Reinen, D. *Inorg. Chem.* **1986**, *25*, 519–522.
(75) García-Lastra, J. M.; Aramburu, J. A.; Barriuso, M. T.; Moreno, M. *Phys. Rev. Lett.* **2004**, *93*, 226402–1–4.
(76) Opalka, D.; Poluyanov, L. V.; Domcke, W. *J. Chem. Phys.* **2011**, *135*, 104108–1–10.
(77) Mondal, P.; Opalka, D.; Poluyanov, L. V.; Domcke, W. *J. Chem. Phys.* **2012**, *136*, 084308–1–12.
(78) O'Brien, M. C. M. *Proc. R. Soc. London, Ser. A* **1964**, *281*, 323–339.

(79) McLain, S. E.; Dolgos, M. R.; Tennant, D. A.; Turner, J. F. C.; Barnes, T.; Proffen, T.; Sales, B. C.; Bewley, R. I. *Nat. Mater.* **2006**, *5*, 561−566.
(80) Barriuso, M. T.; Aramburu, J. A.; Moreno, M. *J. Phys.: Condens. Matter* **1990**, *2*, 771−777.
(81) Nurullin, G. M.; Galygo, L. N.; Egranov, A. V.; Nepomnyachikh, A. I. *J. Phys.: Condens. Matter* **1991**, *3*, 83−90.
(82) Reynolds, R. W.; Boatner, L. A.; Abraham, M. M.; Chen, Y. *Phys. Rev. B* **1974**, *10*, 3802−3817.
(83) Riley, M. J.; Hall, J.; Krausz, E. R. *Aust. J. Chem.* **2012**, *65*, 1298.